Redox Biology 66 (2023) 102846

Contents lists available at ScienceDirect

Redox Biology

journal homepage: www.elsevier.com/locate/redox

Metabolic reprogramming in inflammatory microglia indicates a potential way of targeting inflammation in Alzheimer's disease

Moris Sangineto [a,1,*], Martina Ciarnelli [a,1], Tommaso Cassano [b], Antonio Radesco [c], Archana Moola [a], Vidyasagar Naik Bukke [a], Antonino Romano [a], Rosanna Villani [a], Hina Kanwal [a], Nazzareno Capitanio [d], Loren Duda [e], Carlo Avolio [f], Gaetano Serviddio [a]

[a] C.U.R.E. (University Center for Liver Disease Research and Treatment), Liver Unit, Department of Medical and Surgical Sciences, University of Foggia, Foggia, Italy
[b] Department of Medical and Surgical Sciences, University of Foggia, Foggia, Italy
[c] Istituto Oncologico "Giovanni Paolo II", I.R.C.S.S. of Bari, Laboratory of Haematological Diagnostics and Cellular Therapy, Bari, Italy
[d] Biochemistry Unit, Department of Clinical and Experimental Medicine, University of Foggia, Foggia, Italy
[e] Pathology Unit, Department of Clinical and Experimental Medicine, University of Foggia, Foggia, Italy
[f] Neurology Unit, Department of Medical and Surgical Sciences, University of Foggia, Foggia, Italy

ARTICLE INFO

Keywords:
Immunometabolism
Alzheimer's disease
Microglia
Dimethyl malonate
Macrophage
Bioenergetics
3xTg-AD mice

ABSTRACT

Microglia activation drives the pro-inflammatory activity in the early stages of Alzheimer's disease (AD). However, the mechanistic basis is elusive, and the hypothesis of targeting microglia to prevent AD onset is little explored. Here, we demonstrated that upon LPS exposure, microglia shift towards an energetic phenotype characterised by high glycolysis and high mitochondrial respiration with dysfunction. Although the activity of electron transport chain (ETC) complexes is boosted by LPS, this is mostly devoted to the generation of reactive oxygen species. We showed that by inhibiting succinate dehydrogenase (SDH) with dimethyl malonate (DMM), it is possible to modulate the LPS-induced metabolic rewiring, facilitating an anti-inflammatory phenotype. DMM improves mitochondrial function in a direct way and by reducing LPS-induced mitochondrial biogenesis. Moreover, the block of SDH with DMM inhibits the recruitment of hypoxia inducible-factor 1 α (HIF-1α), which mediates the induction of glycolysis and cytokine expression. Similar bioenergetic alterations were observed in the microglia isolated from AD mice (3xTg-AD), which present high levels of circulating LPS and brain *toll-like receptor4* (TLR4). Moreover, this well-established model of AD was used to show a potential effect of SDH inhibition *in vivo* as DMM administration abrogated brain inflammation and modulated the microglia metabolic alterations of 3xTg-AD mice. The RNA-sequencing analysis from a public dataset confirmed the consistent transcription of genes encoding for ETC subunits in the microglia of AD mice (5xFAD). In conclusion, TLR4 activation promotes metabolic changes and the pro-inflammatory activity in microglia, and SDH might represent a promising therapeutic target to prevent AD development.

1. Introduction

Alzheimer's Disease (AD) is the most common cause of dementia, a continuous decline in thinking, behavioural and social skills. AD is macroscopically characterised by a cortical atrophy, while on the cellular level, extracellular inflammatory or neuritic (NP) senile plaques can be found, consisting of beta-type amyloid (Aβ) protein aggregates and intracellular neurofibrillary tangles (NFTs) formed by hyperphosphorylated tau protein aggregates [1]. However, microglia, "brain-resident macrophages", have recently emerged as major pathogenic drivers in almost all neurodegenerative diseases, including AD [2]. When activated, microglia adopt an inflammatory phenotype and exert a neurotoxic effect through the release of pro-inflammatory cytokines (i.e. IL-1β, TNF-α and IL-6) and reactive oxygen species (ROS) [2]. Recently, the key role of toll-like receptors (TLRs), and in particular TLR4, in neurodegenerative diseases, including AD, has emerged [3,4]. In the brain, TLR4 is mainly expressed on the surface of microglia, and in AD its expression increases in parallel with accumulation of Aβ, leading

* Corresponding author.
E-mail addresses: moris.sangineto@unifg.it, moris.sangineto@gmail.com (M. Sangineto).
[1] These authors contributed equally.

https://doi.org/10.1016/j.redox.2023.102846
Received 17 July 2023; Accepted 8 August 2023
Available online 9 August 2023

to microglia activation with consequent inflammation, neuronal dysfunction and further Aβ and tau deposition [5]. Therefore, although TLR4 is conventionally considered the key receptor for LPS recognition [6,7], it seems to be also involved in phagocytosis and removal of Aβ plaque [8,9]. On the other hand, high levels of LPS have been found in the blood and in the brain of AD patients, so that LPS has been proposed as a mediator between gut dysbiosis and amyloid pathology [10,11]. Overall, these findings have suggested to target TLR4 in preclinical studies, showing some beneficial effects in terms of neuronal inflammation and oxidative stress [12]. However, despite the promising results, the translational approach is not feasible yet and the research of other interacting factors is needed. Recent evidence reported that TLR4-mediated inflammatory activity seems to be fuelled by a metabolic reprogramming as LPS-activated microglia rely on glycolysis, and cytokine production increases under high-glucose conditions [6,7]. In accordance, glucose seems to be the main energy source for microglia in AD, although other substrates can be also used [8]. In this regard, studies of immunometabolism shed light on the importance of metabolic reprogramming as a driving force of pro-inflammatory activation and cell differentiation in immune cells, including macrophages [9]. It is conventionally known that activated M1 macrophages rely on glycolytic metabolism to supply the pro-inflammatory activity, while oxidative phosphorylation (OXPHOS) would represent the main energy source of resting and regulatory phenotypes (e.g. M2 macrophages or Treg lymphocytes) [13–15]. Since the TLR4-mediated activation of microglia reflects an important player in AD, we investigated the role of microglia immunometabolism by dissecting cellular bioenergetics in LPS-activated human microglia, and studying potential applications in a well-established murine model of AD.

2. Material and methods

2.1. HMC3 culture

HMC3 human microglia cell line (ATCC®) was cultured in Eagle's Minimum Essential Medium (Corning) supplemented with 10% of fetal bovine serum (FBS) and 1% penicillin and streptomycin (P/S; Sigma Aldrich) in 6 well-plates with $2x10^5$ cells per well.

2.2. Stimulation of HMC3

As reported by ATCC® and recent studies, the human cell line HMC3 retains the properties of primary microglial cells [16–18], and expresses also more specific microglial markers recently described [19], representing a valid system for biochemical and functional studies of microglia. This permitted to study pathogenetic mechanisms in human cells and to overcome the necessity of killing a large number of animals to have sufficient primary cells for the several studies performed. Therefore, animal model and primary cells analysis were used to give a translational meaning to the work.

After seeding in 6 well-plates, HMC3 cells were stimulated with LPS (1 μg/mL) (*Escherichia coli* O111:B4, Sigma-Aldrich) and simultaneously treated with dimethyl malonate (DMM) (10 mM) (Sigma-Aldrich) for 24 h prior to perform bioenergetic analyses and isolate RNA, proteins or mitochondria. To evaluate the role of TLR4 in the cytokine production, HMC3 cells were stimulated with TAK-242 (Cayman chemical), a specific inhibitor of TLR4 signalling, at 1 μM concentration for 1 h prior to the addition of LPS. Moreover, the role of *Hypoxia-inducible factor-1α* (HIF-1α) and its link with succinate dehydrogenase (SDH) was firstly studied by stimulating with LPS (1 μg/mL) +/- S-2-amino-3-[4′-N,N,-bis (2-chloroethyl) amino]-phenyl propionic acid N-oxide dihydrochloride (PX-478) (Cayman chemical), a HIF-1α inhibitor, at 10 μM concentration for 24 h, and in a second step, with diethyl succinate (here indicated as Succ) (5 mM) for 3 h prior to add LPS (1 μg/mL) and DMM (10 mM) for 24 h. β-Amyloid peptide (1-42) ($Aβ_{1-42}$) was prepared according to manufacturer's protocol, diluted in calcium and magnesium-free PBS and incubated for 24 h at 37∘C to pre- aggregate the peptides. Then, HMC3 were stimulated with $Aβ_{1-42}$ (10 ug/mL), after testing different concentrations (Supplementary Fig. 1), for 24 h ± a pre-treatment for 1 h with TAK-242 (1 μM). In another experimental setting it was analysed the effect of long-lasting exposure with LPS (1 μg/mL), every day for 10 days, +/- DMM (10 mM) the last day only. Doses and administration times of DMM, TAK-242, diethyl succinate and Aβ were selected based on other relevant articles [9,20,21] and/or testing different concentrations, as shown in Supplementary Figs. 1 and 2.

2.3. Animal experimental model

6- and 18-month-old male Non-Tg (n= 29) and 3xTg-AD (n= 50) mice with 3 mutant human genes (APP_{Swe}, PS_{1M146V} and tau_{P301L}) were used for *in vivo* and *ex vivo* studies. The 3xTg-AD mice have been genetically engineered by LaFerla and colleagues at the Department of Neurobiology and Behaviour, University of California, Irvine. Colonies of homozygous 3xTg-AD and Non-Tg mice were established at the University of Foggia, Italy. This model exhibits AD-like plaques and tangles associated with synaptic dysfunction [22–26]. The 3 × Tg-AD mice background strain is a C57BL6/129SvJ hybrid, and genotypes were confirmed from tail biopsy. Mice were intraperitoneally injected with DMM (160 mg/kg) [20] or vehicle, Dulbecco's Phosphate Buffered Saline (PBS), once a day for 3 days, and then sacrificed. Mice were raised under 22 °C temperature, 12/12-h light/dark cycle and ad libitum access to fresh food and water. Mice brain cortex was collected for histological and molecular studies, while another court was used for freshly isolation of microglia. All the experiments were performed in accordance with the Italian National Laws (DL 116/92) and the European Communities Council Directives (86/609/EEC).

2.4. Microglia isolation from mice brains

Microglia cells were freshly obtained from the cerebral cortices of 6- and 18-month-old Non-Tg or 3xTg-AD mice, as previously reported [27] with some modifications. Meninges and cerebellum were carefully removed, and the tissues were triturated with a 15 T scalpel blade in ice-cold Dulbecco's Modified Eagle Medium/Nutrient Mixture F-12 (DMEM/F12; Sigma) containing 1% P/S and 1% of Glucose (Sigma Aldrich). Minced brains were transferred to a 50 ml falcon tube containing a dissociation medium (HBSS 1X; Sigma with 20 U/ml DNase I and 2 mg/ml collagenase) and the tube was gently inverted in a cell incubator at 37 °C for 20 min. After two sequential centrifugation pellet was resuspended in DMEM/F12 medium. A cell suspension was obtained by pipetting up and down with a serological pipette against the bottom of tube until large clumps of tissue were broken up and thereafter by passing the cell solution through a 70 μm cell-strainer. Microglia separation from myelin was achieved using a 30% Percoll solution; the pellet containing microglial cells was resuspended in culture medium (DMEM/F12 with 10% FBS and 1% P/S) and plated on T-25 flasks (for mRNA isolation) or in Seahorse-96-well plate, for bioenergetic analysis ($1 x 10^5$ cells per well). After a 1-h incubation at 37 °C in a humidified 5% CO_2 incubator, culture medium was removed and replaced with a fresh one to remove floating debris.

2.5. Measurement of Real-Time ECAR and OCR

Real-time extracellular acidification rate (ECAR) and oxygen consumption rate (OCR) were measured using a Seahorse XFe96 analyser (Agilent, Santa Clara, US) according to the manufacturer's instructions, with minor modifications. $2 x 10^5$ HCM3 cells or $1 x 10^5$ primary isolated microglia were plated on the XFe96 cell culture microplate and cultured as indicated. The utility plate was hydrated with sterile water (200 μl/well) and incubated overnight (37 °C, CO_2-free). The day after, the sterile water was replaced with XF calibrant solution (pH 7.4) (200 μl/well) and incubated for 1h at 37 °C in a CO_2-free incubator. Then, the

utility plate with the cartridge containing injector ports and sensors was run on the Seahorse for calibration. Consequently, the utility plate was removed, and the cartridge positioned on the cell plate for analysis. The assay medium (Seahorse XF DMEM assay medium, pH 7.4) was prepared immediately before assay. For ECAR and OCR measurements in HMC3, in all experimental settings the exposure to molecules was performed for 24 h, then the medium replaced before loading the plate into the Seahorse XFe96 analyser. OCR was measured under basal conditions and after sequential injection of specific inhibitors: oligomycin A (1 μM), carbonyl cyanide-p-trifluoromethoxy phenylhydrazone (FCCP) (1 μM) and rotenone/antimycin A (1 μM). Oligomycin A stops ATP-synthase, permitting to evaluate the quote of respiration addressed to ATP production; the FCCP is an uncoupler which dissipates proton gradient and allow to measure the maximal respiratory capacity. Rotenone/Antimycin A (complex I and III inhibitors, respectively) are finally injected in order to block electron transport chain (ETC), measuring the non-mitochondrial respiration level. ECAR was measured under basal conditions and after sequential injection of oligomycin A (1 μM) and 2-deoxy-glucose (2-DG) (50 Mm). Oligomycin A boosts glycolysis blocking mitochondrial ATP production, permitting to evaluate the glycolysis capacity. 2-DG inhibits glycolysis. Analysis was performed using Wave software.

2.6. qPCR

Total RNA was isolated from cultured HMC3 and mice frozen brain cortices using QIAzol Lysis Reagent (Qiagen). Equal amounts of RNA were reverse transcribed to cDNA using a high-capacity cDNA reverse transcription kit (Applied Biosystems) according to the manufacturer's instructions. Real-time PCR was performed, using Sso Advanced universal SYBR green supermix on a Bio-Rad CFX96 Real-Time system as previously reported [13,28]. The cycle threshold (Ct) was determined and the relative gene expression was calculated with the ΔΔCT method. The gene expression was normalized to human or mouse β-actin. Primers are listed in Table 1 in Supplementary.

2.7. Western blot analysis

A standard protocol was used to perform Western blot analysis (Bio-Rad Laboratories). Lysates from HMC3 were prepared in RIPA lysis buffer containing phosphatase and protease inhibitors. Lysates with equal amounts of protein (40 μg) were loaded in an 8% SDS-PAGE, transferred to a nitrocellulose membrane (Bio-Rad) and blocked with 5% bovine serum albumin (BSA) in Tris-buffered saline containing 0.1% Tween-20 (TBST) for 1 h at room temperature. Then, membranes were incubated overnight at 4 °C with these following primary antibodies: HIF-1α (1:1000, Cell Signaling Technology) and β-actin (1:1000, Sigma-Aldrich), as loading control. Therefore, membranes were incubated with the appropriate HRP-conjugated secondary antibody (Cell Signaling Technology) for 1 h at room temperature and bands were detected by the ClarityTM Western ECL Blotting Substrate using a ChemiDoc MP system (Bio-Rad Laboratories Inc, Segrate (MI), Italy) and quantified by the Image LabTM Software.

2.8. Preparation of mitochondria-enriched fractions for mitochondrial complexes enzymatic activity

The mitochondria-enriched fractions from cell suspension were prepared as previously reported [13,28–30] with minor adjustments. Briefly, cells were washed with ice-cold phosphate-buffered saline and centrifuged at 3500 rpm for 6 min at 4 °C. Supernatant was carefully removed and the cell pellet was resuspended in 10 mM/L Tris, pH 7.6, with protease and phosphatase inhibitors (Sigma-Aldrich), freeze thawed three times in liquid nitrogen. Cells were also mechanically disrupted with a 2-mL glass/teflon potter on ice. The concentration of mitochondria enriched cell suspension was estimated by Bradford assay. The purity check was performed by western-blot, staining proliferating cell nuclear antigen (PCNA) (Cell signaling, 1:1000), cytochrome *c* (Cell signaling, 1:1000) and α-tubulin (Cell signaling, 1:1000), as nuclear, mitochondrial and cytosolic marker, respectively.

2.9. Complex I assay

Complex I enzymatic activity was measured spectrophotometrically at 600 nm as previously reported [13,28,29]. Briefly, 40 μg of each enzyme solution was mixed with complex I buffer (25 mM/L potassium phosphate, 3.5 g/L fatty acid free BSA), 60 μM/L 2,6-Dichlorophenolindophenol (DCPIP), 70 μM/L decylubiquinone (DBH), 1.0 μM/L antimycin-A) and incubated for 3 min at 37 °C. Then, we added 10 mM/L NADH and measured the absorbance for 4 min at 37 °C. Later, the reference was measured in the presence of 2.5 μM rotenone. Enzyme activity was calculated with molar extinction coefficient (ε) for the DCPIP (19.1 mM^{-1} cm^{-1}).

2.10. Complex II assay

Complex II enzymatic activity was measured spectrophotometrically at 600 nm as previously reported [13,28,31]. Briefly, 40 μg of each cell suspension was incubated with complex II buffer (25 mM KH_2PO4 (pH 7.8), 2 mM EDTA, 1 mg/mL fatty acid free BSA), 10 mM succinate, 50uM DBH, 1 mM KCN, 4 μM rotenone, and 10 μM antimycin A, 0.2 mM ATP) for 10 min. After the addition of 80 μM DCPIP, the change in absorbance at 600 nm was recorded for 2 min for reference. The addition of 10 mM malonate inhibits the oxidation of succinate. Enzyme activity was calculated with ε for the DCPIP (19.1 mM^{-1} cm^{-1}).

2.11. Complex V (ATP-synthase) assay

Complex V enzymatic activity was measured spectrophotometrically at 340 nm[13, 28, 31]. Complex V buffer (50 mM Tris-Hcl (pH 8.0), 5 mg/mL BSA), 20 mM $MgCl_2$, 50 mM KCl, 1 mM NADH, 10 mM phosphoenolpyruvate, 5 μM antimycin A, 15 μM Carbonylcyanide3-chlorophenylhydrazone), 4 units of lactate dehydrogenase, and pyruvate kinase were incubated with 2.5 mM ATP for 2 min. After this, 40 μg of each mitochondria cell suspension was added to the above mixture, and the change in absorbance at 340 nm was recorded for 5 min. The reference was measured in the presence of 3 μM oligomycin for 5 min. Enzyme activity was calculated with ε for the NADH (6.22 mM^{-1} cm^{-1}).

2.12. Measurement of H_2O_2 production

The rate of peroxide production was determined in mitochondrial-rich cell suspension prepared as mentioned above using Amplex red as previously reported [28,32]. Briefly, mitochondrial H_2O_2 production was measured at 37 °C following the oxidation of Amplex Red by horseradish peroxidase in mitochondria rich cell suspension using 5 mM pyruvate plus 1 mM malate or 5 mM succinate as respiratory substrates. The fluorescence of supernatants was measured using 530 nm as excitation wavelength and 590 nm as emission wavelength in filter max F5 multimode microplate reader (Beckman Coulter; DTX 880 Multimode Detector). The rate of peroxide production was calculated using a standard curve of H_2O_2.

2.13. Mitochondrial HNE- and MDA-adducts

4-hydroxy-2-nonenal (HNE) and malondialdehyde (MDA) fluorescent adducts formed with mitochondrial proteins in cell suspension were monitored by spectrofluorimetry as previously reported [28,32,33]. Briefly, the mitochondria-enriched fractions from cell suspension were pipetted in 10 mL glass-tube and a volume of ethanol/ether was added. The tubes were vortexed, incubated on ice for 5 min and then centrifuged at 3000 rpm for 5 min. The solvents were discarded, and these

steps were repeated once. The obtained pellet was dissolved in distilled water and the fluorescence intensity of the solution was measured at an emission wavelength of 460 nm and an excitation of 390 nm for MDA-adducts and 355 nm for HNE-adducts. Relative fluorescence units were calculated against a standard quinine sulphate solution (0.1 pg/ml of 0.1 N sulfuric acid).

2.14. TLR4 immunohistochemistry

For immunohistochemistry, brains were stored in 4% PFA for 24 h. After deparaffinization of slides in xylene and dehydration in an ethanol gradient, the antigen was retrieved through a 30 min incubation in a sodium-citrate buffer (pH = 6) in a microwave; to quench endogenous peroxidase activity, sections were incubated with peroxidase blocking reagent (3% H_2O_2 in methanol) for 10 min and rinsed with H_2O for 5 min. Then a protein blocking was executed with Protein Block ready to use (Spring Bioscience). Primary mouse antibody for TLR4 (ab22048; abcam) was diluted in Antibody Diluent Reagent Solution (invitrogen) and incubated overnight at 4 °C, followed by incubation with anti-mouse secondary antibody for 1 h. Finally, the sections were incubated for 30 min with R.T.U. Vectastain®, stained with DAB (Dako, Santa Clara, CA) and counterstained with hematoxylin (Leica Biosystem). The TLR4 positivity was quantified with Fiji software (ImageJ, NIH).

2.15. Immunofluorescence staining for F4/80

Primary microglia were seeded in a chamber slide system with $3x10^4$ cells per each well. Cells were fixed with 4% formaldehyde for 15 min at room temperature, washed twice with PBS and blocked with 5% bovine serum albumin (BSA) for 1 h. Cells were subsequently incubated overnight at 4 °C with the following primary antibody: F4/80 (1:400; Cell Signaling Technology). Cells were then washed three times with PBS and incubated with the secondary antibody Alexa Fluor 488 goat anti-rabbit (1:250, Alexa, Thermo Fisher scientific), for 1 h at room temperature in the dark. Cells were washed three times with PBS and the nuclei were stained with TO-PRO-3 diluted in PBS (1:1500, invitrogen-Molecular Probe, Thermo Fisher scientific). Then, cells were scanned using a Leica confocal microscope with a 40X oil immersion objective (Supplementary Fig. 5).

2.16. Circulating LPS measurement

Circulating LPS in mice serum was determined using Pierce™ Chromogenic Endotoxin Quant Kit (Thermo Fisher scientific), an endpoint amebocyte lysate assay that quantifies endotoxins (LPS). Briefly, according to the manufacturer's protocol, serum was collected from clotted blood, centrifuged at 1300g for 15 min and then stored at −20 °C. Serum samples were 1:50 diluted with endotoxin-free water and subsequently heated to 70 °C for 15 min to inactivate inhibitory proteins. The amount of LPS was quantified by the addition of a chromogenic substrate; the activated protease, catalyzed the release of p-nitroaniline (pNA), spectrophotometrically detected at 405 nm. LPS levels (EU/mL) were calculated based on the standard curve.

2.17. RNA-sequencing analysis

RNA-sequencing (RNA-seq) data were analysed from public repository GSE231403 (https://www.ncbi.nlm.nih.gov/geo/query/acc.cgi?acc=GSE231403). The RNA-seq data of microglia isolated from 3 wild type (WT) mice and 3 5xFAD mice were downloaded: GSM7273528, GSM7273529, GSM7273531, GSM7273535, GSM7273536, GSM7273537 rna.seq raw data were downloaded from NCBI Gene Expression Omnibus (GEO). Raw.tab data were downloaded for each sample and expression values were calculated and normalized (TMM: Trimmed Mean of M component) in R (version 4.1.3) using limma package (version 3.50.3). Differential gene expression was carried out by using the limma package (version 3.50.3) by fitting a linear model of WT vs 5xFAD samples. Following, DEGs were screened out through cut-off criteria of Log fold change between −1 and 1, and -log10 (p value) > 1.3. The graphical representation of differentially expressed genes (DEGs) has been performed with package ggplot2 (version 3.4.2) of R; hence through Volcano plot we have visualized DEGs between WT vs 5xFAD microglia.

A Gene ontology (GO) enrichment analysis has been performed by using goana function of limma package (version 3.50.3), permitting to screen the over-representation of gene ontology (GO) terms (for up-regulated genes). GO analysis included the three categories: BP (Biological process), MF (Molecular Function) and CC (Cellular Component).

2.18. Statistical analysis

GraphPad PRISM v8 was used for statistical analysis. Unpaired two-tailed Student's t-test and one-way analysis of variance followed by post hoc Bonferroni test were used when appropriate. Results are shown as mean ± standard error of mean (SEM). Data were considered statistically significant when $p < 0.05$.

2.19. Software

GraphPad PRISM v8 was used for statistical analysis and graphing. Biorender.com was used to draw the graphical abstract. TLR4 immunostaining was quantified with Fiji software (ImageJ, NIH), while western blot intensities were calculated with Image LabTM Software (Bio-Rad Laboratories Inc). R (version 4.1.3) was used for RNA-seq analysis.

3. Results

3.1. Succinate dehydrogenase (SDH) inhibition controls LPS-induced metabolic rewiring and cytokine expression

HMC3 was activated by LPS exposure for 24 h. In order to analyse the role of metabolic modulation in the control of microglia inflammatory activity, HMC3 cells have been treated with dimethyl malonate (DMM), a succinate dehydrogenase (SDH) inhibitor with demonstrated immunomodulatory properties in macrophages [34,35]. First, we found that pro-inflammatory cytokines, *Interleukin-1β* (IL-1β) and *Tumor necrosis factor-α* (TNF-α), were transcriptionally upregulated in LPS-polarized cells, while a significant down-regulation was found when cells were treated with DMM (Fig. 1A). Moreover, DMM normalized the *Nitric oxide synthase 2, inducible/Arginase 1* (iNOS/Arg1) expression ratio, confirming that SDH inhibition facilitated a M2 macrophagic marker preponderant expression (Fig. 1B). Analysing cellular bioenergetics and measuring glycolysis by extracellular acidification rate (ECAR) (Fig. 1C), we found that LPS considerably increased glycolysis, which was instead normalized by DMM (Fig. 1D). The injection of oligomycin, a mitochondrial ATP-synthase inhibitor, showed a considerable increase of glycolytic capacity in LPS-exposed cells, partially and significantly contrasted by DMM treatment (Fig. 1E). Mitochondrial respiration was determined by OCR at basal state and after inhibitors injection (i.e., oligomycin, FCCP and rotenone/antimycin A) (Fig. 1F). LPS significantly increased basal respiration compared to control, and the estimation of maximal respiration (obtained by the injection of the uncoupler FCCP) was also considerably higher in LPS-stimulated cells (Fig. 1G and H). The block of ATP-synthase with oligomycin, that permits to estimate the quote of respiration linked to ATP production, highlighted that the mitochondrial respiration gain observed in LPS-stimulated cells was not completely finalised to ATP synthesis and entailed a significant proton leak (Fig. 1I). Interestingly, the treatment with DMM partially and significantly reduced the LPS-induced basal and maximal respiration increase, with the consequent leak limitation

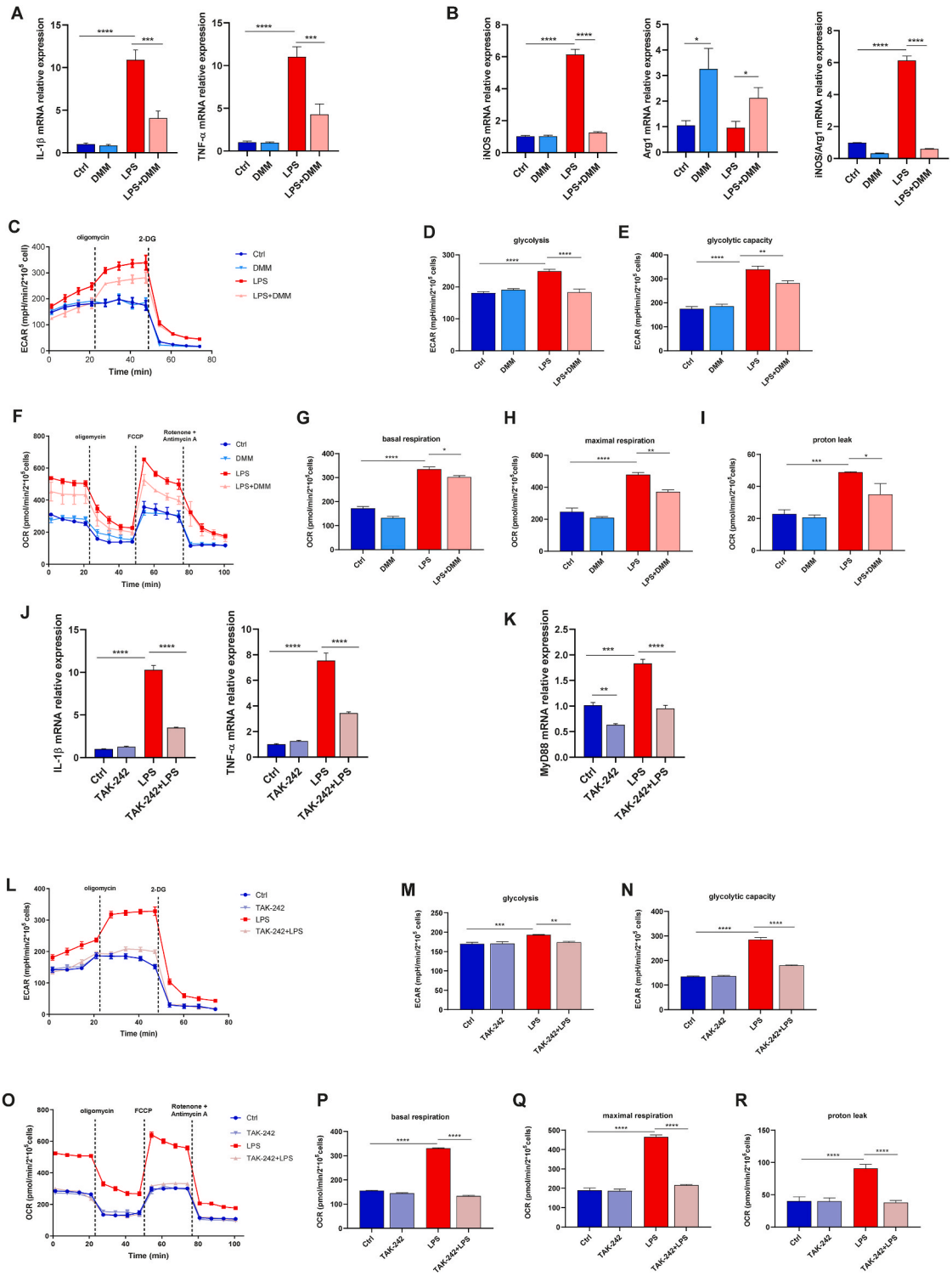

Fig. 1. SDH inhibition with DMM controls LPS-induced metabolic rewiring

(A and B) Relative mRNA expression of pro-inflammatory cytokines (IL-1β and TNF-α) and M1, M2 macrophage markers (iNOS, Arg1 and iNOS/Arg1 ratio) in HMC3 treated with LPS (1 μg/mL) and DMM (10 mM) for 24 h determined by qPCR (n= 5 experiments performed in triplicate). (C–E) Glycolysis determined by measuring ECAR and (F–I) mitochondrial respiration determined by measuring OCR in HMC3 treated with LPS (1 μg/mL) and DMM (10 mM) for 24 h (n= 4 experiments performed in quadruplicate). (J) Relative mRNA expression of pro-inflammatory cytokines (IL-1β and TNF-α) and (K) TLR4 tag, MyD88 in HMC3 pre-treated with TAK-242 (1 μM) for 1 h prior to LPS stimulation (1 μg/mL) for 24 h or treated with simple TAK-242 (1 μM) and LPS (1 μg/mL) for 24 h determined by qPCR (n= 5 experiments performed in triplicate). (L) Glycolysis determined by measuring ECAR and (M) mitochondrial respiration determined by measuring OCR in HMC3 pre-treated with TAK-242 (1 μM) for 1 h prior to LPS stimulation (1 μg/mL) for 24 h or treated with simple TAK-242 (1 μM) and LPS (1 μg/mL) for 24 h (n= 4 experiments performed in quadruplicate). Data are expressed in mean ± SEM; *p < 0.05; **p < 0.01; ***p < 0.001, ****p < 0.0001 according to one-Way ANOVA followed by post hoc analysis (Bonferroni test). Il-1β, interleukin-1β; TNF-α, tumor necrosis factor-α; iNOS, inducible nitric oxide synthase; Arg1, arginase1; MyD88, MYD88 innate immune signal transduction adaptor; LPS, lipopolysaccharide; DMM, dimethyl malonate; ECAR, extracellular acidification rate; OCR, oxygen consumption rate.

(Fig. 1F–I). Overall, these results showed that upon LPS activation, microglia metabolically switch to an energetic phenotype characterised by an "hypermetabolic state" as aerobic glycolysis and mitochondrial respiration increase to support ATP production, although with a considerable proton leak. SDH inhibition with DMM controls LPS-induced metabolic rewiring, inhibiting cytokine production. In a second step, in order to confirm that LPS-induced microglia activation and cytokine production effectively depended on TLR4, HMC3 were pre-treated with TAK-242, a specific inhibitor of TLR4 signalling [36]. As expected, treatment with TAK-242 almost abrogated the LPS-induced expression of pro-inflammatory cytokines (i.e., IL-1β and TNF-α) (Fig. 1J). Accordingly, the expression of *MYD88 innate immune signal transduction adaptor* (MyD88), an important intracellular TLR4 adaptor molecule, was normalized by TAK-242 despite the LPS exposure (Fig. 1K). To further corroborate the link between the LPS-TLR4 signaling, metabolic reprogramming and inflammatory activity, we evaluated the bioenergetic profile of HMC3 with TAK-242 exposure, observing that TLR4 inhibition perfectly nullified the metabolic reprogramming induced by LPS, both in terms of glycolysis and mitochondrial respiration (Fig. 1 L–R).

Finally, considering the above-mentioned studies that indicate a role of Aβ in activating microglia via TLR4 [8,12], we have also analysed the effects of $A\beta_{1\text{-}42}$ exposure in microglia. To do this, HMC3 cells were exposed to $A\beta_{1\text{-}42}$ for 24 h, with or without TLR4 inhibitor (TAK-242), finding a transcriptional upregulation of IL-1β and TNF-α in $A\beta_{1\text{-}42}$-stimulated cells, although in less extent compared to LPS stimulation (Supplementary Fig. 3A). Interestingly, cytokine and MyD88 expression was abrogated in presence of TAK-242, suggesting that Aβ exert a pro-inflammatory activity via TLR4. (Supplementary Figs. 3A and B). Moreover, similarly to LPS, $A\beta_{1\text{-}42}$ treatment reprogrammed cellular metabolism increasing glycolysis and mitochondrial respiration, and TAK-242 restored the normal bioenergetic profile, corroborating again the role of TLR4 (Supplementary Figs. 3C–I). Along these lines, we might speculate that Aβ acts as a microglia activator via TLR4, although relatively weak compared to LPS both in terms of cytokine expression and metabolic reprogramming. Increasing the dosage of Aβ did not change the proinflammatory effect (Supplementary Fig. 1C).

3.2. SDH inhibition reduces the LPS-induced mitochondrial dysfunction and biogenesis

As described above, LPS exposure induced high glycolysis levels and high mitochondrial respiration with consequent proton leak. Moreover, DMM limited these metabolic changes and reduced cytokine expression, suggesting that both glycolysis and oxidative stress (derived from mitochondrial dysfunction) could play a role in the TLR4-mediated inflammation. To clarify this, we added different amounts of glucose or H_2O_2 to the culture medium of LPS-DMM-treated cells. Intriguingly,

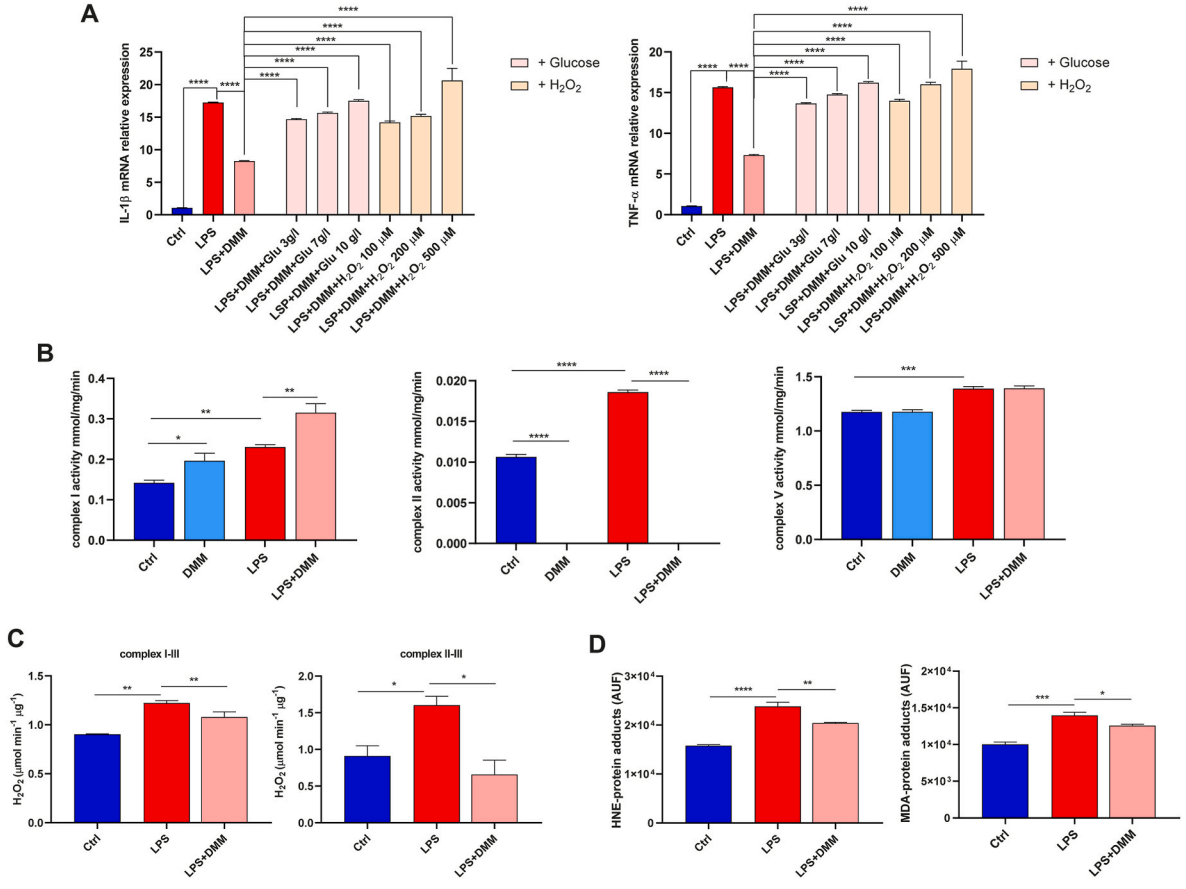

Fig. 2. SDH inhibition with DMM reduces mitochondrial dysfunction and oxidative stress
(A) Relative mRNA expression of pro-inflammatory cytokines (IL-1β and TNF-α) in HMC3 treated with LPS (1 μg/mL) and DMM (10 mM) and with increasing concentrations of glucose (3 g/L, 7 g/L, 10 g/L) and H_2O_2 (100 μM, 200 μM, 500 μM) for 24 h determined by qPCR (n= 3 experiments performed in triplicate). (B) Respiratory chain Complexes I, II, V enzymatic activity determined spectrofotometrically in HMC3 after 24 h treatment with LPS (1 μg/mL) and DMM (10 mM) (n= 3 experiments performed in triplicate). (C) Peroxide production from pyruvate/malate (complex I-III) and succinate (complex II-III), in HMC3 after 24 h treatment with LPS (1 μg/mL) and DMM (10 mM) (n= 3 experiments performed in triplicate). (D) Mitochondrial levels of MDA- and HNE-protein adducts in HMC3 after 24 h treatment with LPS (1 μg/mL) and DMM (10 mM) (n= 3 experiments performed in triplicate). Data are expressed in mean ± SEM; *p < 0.05; **p < 0.01; ***p < 0.001, ****p < 0.0001 according to one-Way ANOVA followed by post hoc analysis (Bonferroni test). Il-1β, interleukin-1β; TNF-α, tumor necrosis factor-α; LPS, lipopolysaccharide; DMM, dimethyl malonate; MDA, malondialdehyde; HNE, 4-hydroxynonenal.

we observed that the DMM anti-inflammatory effect was progressively abolished by increasing the concentrations of glucose and H_2O_2 (Fig. 2A), confirming that both glycolysis and oxidative stress are involved in TLR4-mediated cytokine production. Therefore, in the second step, we dissected the LPS-induced mitochondrial dysfunction by analysing the ETC enzymatic activity and the H_2O_2 production rate. The analysis revealed that LPS significantly enhanced the activity of complex I and complex II, while DMM inhibited complex II activity to undetectable levels. In contrast, complex I activity was further increased by DMM (Fig. 2B). No difference was found in complex V activity that was higher in both LPS and LPS+DMM compared to the control (Fig. 2B). However, we quantified the H_2O_2 production rate by using pyruvate/malate (complex I-III) and succinate (complex II-III) as mitochondrial substrates, revealing that DMM treatment restored to normal levels the LPS-induced peroxide production (Fig. 2C). Accordingly, MDA- and HNA-protein adducts amount resulted significantly higher in LPS-activated microglia and partially normalized in DMM-treated cells (Fig. 2D). Taken together, these results underlined that TLR4-mediated cytokine expression in microglia required the enhancement of mitochondrial respiration with consequent radical oxygen species (ROS) production, which were efficiently counteracted by targeting SDH with DMM. Moreover, it was interesting to note that LPS exposure induced mitochondrial biogenesis as demonstrated by the higher expression of markers such as *Transcription factor A, Mitochondrial* (TFAM) and *Peroxisome Proliferator-Activated Receptor Gamma, Coactivator 1 Alpha* (PGC-1α) (Fig. 3A and B), and several mitochondrial subunits such as *NADH:ubiquinone oxidoreductase subunit A1* (NDUFA1), *NADH:ubiquinone oxidoreductase subunit A8* (NDUFA8), *NADH:ubiquinone oxidoreductase subunit B3* (NDUFB3), *Succinate dehydrogenase complex iron sulfur subunit B* (SDHB), *Cytochrome c oxidase subunit 4I1* (COX4I1), *Cytochrome c oxidase subunit 5B* (COX5B), *Cytochrome c oxidase subunit 6A1* (COX6A1) *and ATP synthase membrane subunit c locus 2* (ATP5G2) (Fig. 3C). The treatment with DMM restored the expression of TFAM, PGC-1α, and ETC subunits, suggesting that probably DMM controlled the mitochondrial activity not only by direct inhibition of SDH but also by through inhibiting mitochondrial biogenesis.

3.3. Cytokine expression is mediated by HIF-1α

Previous studies have demonstrated that HIF-1α plays a crucial role in LPS-induced cytokine production and that succinate and SDH activity are modulators of HIF-1α activity [37–39]. In accordance with this, we observed a considerable increase of HIF-1α protein level in LPS-stimulated HMC3 cells, which was abolished by DMM administration (Fig. 4A), hence suggesting a role of HIF-1α and a link with SDH activity. To corroborate this, we treated LPS-exposed cells with PX-478 (10 μM), a HIF-1α specific inhibitor [40,41], showing a down-regulation of both Il-1β and TNF-α expression (Fig. 4B). Interestingly, comparing PX-478 and DMM effects we found a comparable IL-1β and a similar TNF-α down-regulation (Fig. 4B). As already demonstrated, HIF-1α transcripts for glycolysis enzymes contributing to increase glycolysis in LPS-stimulated macrophages [15,42]. Therefore, we supposed that SDH inhibition might limit glycolysis via HIF-1α. In accordance, we found that the inhibition of HIF-1α with PX-478, similarly to DMM, was able to reduce glycolytic capacity in LPS-exposed microglia, although with no significant effects on basal glycolysis (Fig. 4C). To further clarify the relation between HIF-1α and SDH activity, we treated cells with cell-permeable diethyl succinate [20], in order to provide supplementary substrates to SDH by increasing mitochondrial levels of succinate. We found that succinate increased HIF-1α when administered alone, and contrasted the DMM-induced HIF-1α reduction (Fig. 4D).

3.4. SDH inhibition dampens brain inflammation in 6-month-old 3xTg-AD mice

Since the AD is associated with a chronic inflammation and microglia activation plays a pivotal role in this neurodegenerative disorder [43], we used 3xTg-AD mice, an AD model harboring three mutant genes: β-amyloid precursor protein (βAPP_{Swe}), presenilin-1 (PS_{1M146V}) and tau_{P301L}. The 3xTg-AD mice develop Aβ and tau pathologies in age-dependent manner, mimicking the human AD brain profile [23,44–46]. Some studies suggest that TLR4 is a key receptor on microglia, since it could be involved in the production of pro-inflammatory cytokines in AD pathology and cognitive impairment [3,4]. We corroborated this finding by staining TLR4 in 3xTg-AD mice cortex that showed higher levels compared to Non-Tg mice (Fig. 5A). Moreover, it was previously demonstrated that LPS, the main TLR4 ligand, is significantly high in the blood of AD patients [11], so that LPS has been proposed as a mediator between gut dysbiosis and amyloid pathology [10]. Interestingly, we have quantified circulating LPS in 3xTg-AD mice serum, finding a significant increase compared to Non-Tg mice (Fig. 5B). To investigate whether DMM could also exert an *in vivo* immunomodulating effect in AD, 3xTg-AD 6-month-old mice were intraperitoneally injected with DMM at 160 mg/kg or vehicle (PBS) once a day for three days (Fig. 5C). Interestingly, DMM-treated 3xTg-AD mice presented a significant reduction of cortex TNF-α expression, while IL-1β expression was even abrogated (Fig. 5D). Moreover, compared to Non-Tg, vehicle-3xTg-AD mice presented higher transcriptional levels of iNOS/Arg1 ratio, revealing a preponderant expression of a M1 macrophagic marker (Fig. 5D). While, iNOS/Arg1 expression ratio was normalized by DMM, confirming that SDH inhibition facilitated a M2 preponderant expression (Fig. 5D). To confirm that DMM anti-inflammatory effect was due to the metabolic modulation, we isolated microglia from untreated and DMM-treated mice and examined the bioenergetic profile *ex vivo*. As shown by ECAR (Fig. 5E), both glycolysis and glycolytic capacity very considerably increased in 3xTg-AD microglia compared to Non-Tg, and partially restored after DMM treatment (Fig. 5E). Moreover, compared to Non-Tg mice, 3xTg-AD vehicle-mice showed a significant increase of basal and maximal respiration with a very considerable leak, which were instead significantly reduced by DMM injection, although not completely normalized (Fig. 5F). Along these lines we may confirm that microglia, in a well-established AD model, present a TLR4 mediated activation, with a M1 polarization, and similarly to LPS-stimulated cells, show an energetic phenotype characterised by increase of glycolysis and mitochondrial dysfunction. Interestingly, targeting microglia immunometabolism in AD mice with a SDH inhibitor (DMM) was efficient to modulate the bioenergetic profile and abrogate inflammation.

3.5. RNA-seq analysis in WT vs 5xFAD mice confirmed a role of mitochondrial repurposing in microglia

5xFAD transgenic mice overexpress both mutant human Aβ (A4) precursor protein 695 (APP)) with the Swedish (K670 N, M671L), Florida (I716V), and London (V717I) Familial Alzheimer's Disease (FAD) mutations and human presenilin 1 (PS1) harboring two FAD mutations, M146L and L286V [47]. This transgenic model, despite not showing tau accumulation, exhibits a rapid Aβ plaque formation and gliosis. It is described a pro-inflammatory profile until the age of 9 months [47].The analysis of RNA-seq dataset performed on microglia isolated from mice (9 months-aged) brains revealed a very different gene expression profile between WT mice and 5xFAD mice. In particular, the analysis of DEGs identified 2834 down-regulated and 2453 up-regulated genes in 5xFAD microglia. Setting significance criteria of Log fold change between −1 and 1, and -log10 (p value) > 1.3, we obtained 134 significant up-regulated DEGs and 411 down-regulated DEGs in 5xFAD (Fig. 6A) (DEGs list in Supplementary Tables 3 and 4).

Of note, the most up-regulated DEG in 5xFAD microglia was apolipoprotein E (ApoE) (p value = 4.349456e-08, -log10(pvalue) = 7.361565), a gene whose allele ε4 is a known risk factor for AD development [48]. Moreover, it has been shown that ApoE, and in particular its allele ε4, would be implicated in Aβ recognition by TLR4 on microglia [12].

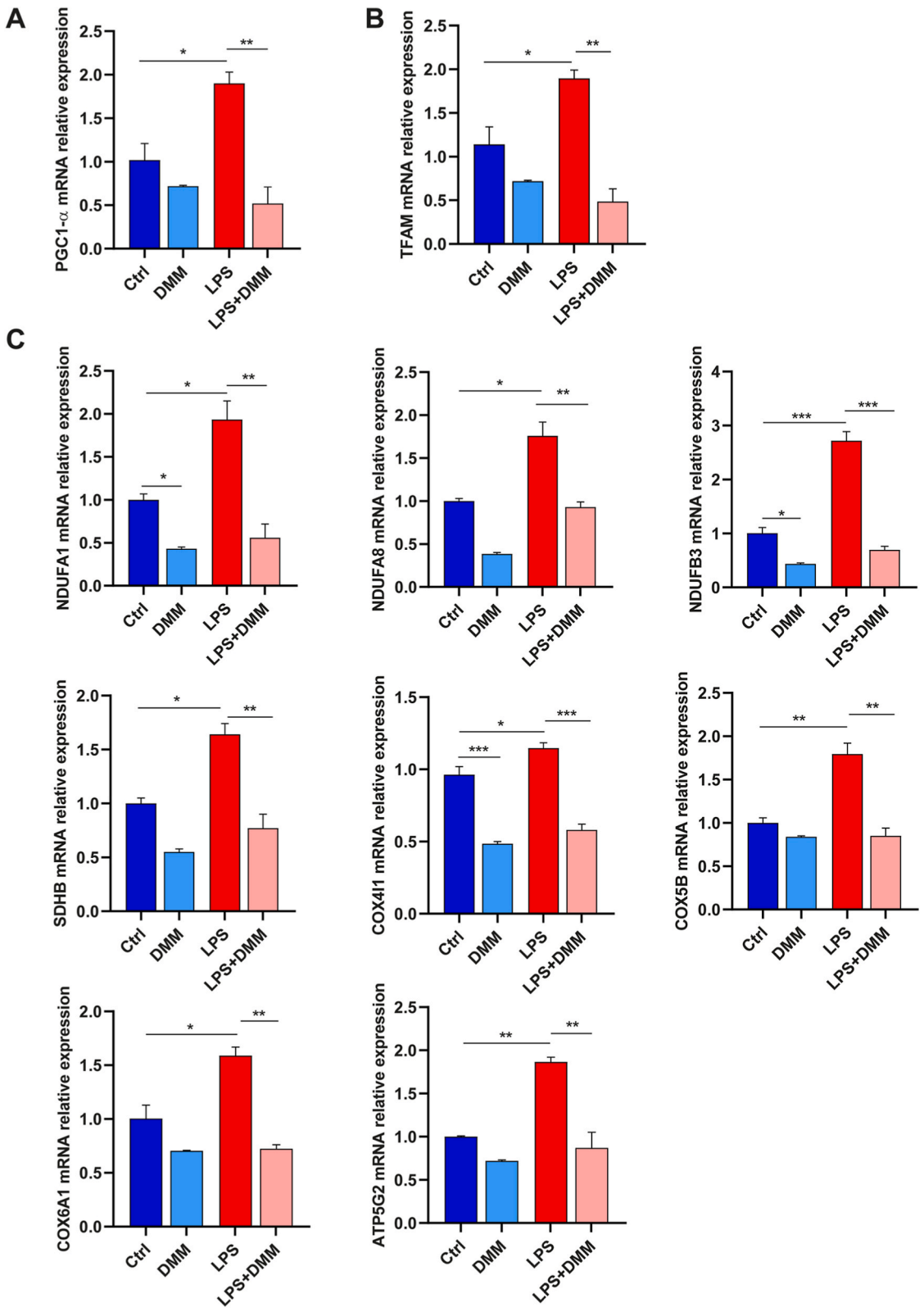

Fig. 3. SDH inhibition limits the LPS-induced mitochondrial biogenesis

(A and B) Relative mRNA expression of markers of mitochondrial biogenesis (TFAM and PGC1-α) and (C) different mitochondrial complexes subunits (NDUFA1, NDUFA8, NDUFB3, SDHB, COX4I1, COX5B, COX6A1, ATP5G2) in HMC3 treated with LPS (1 μg/mL) and DMM (10 mM) for 24 h determined by qPCR (n= 3 experiments performed in triplicate). Data are expressed in mean ± SEM; *p < 0.05; **p < 0.01; ***p < 0.001, according to one-Way ANOVA followed by post hoc analysis (Bonferroni test). TFAM, Transcription Factor A, Mitochondrial; PGC-1 α, Peroxisome proliferator–activated receptor gamma coactivator-1 alpha; LPS, lipopolysaccharide; DMM, dimethyl malonate; NDUFA1, NADH:ubiquinone oxidoreductase subunit A1; NDUFA8, NADH:ubiquinone oxidoreductase subunit A8; NDUFB3, NADH:ubiquinone oxidoreductase subunit B3; SDHB, Succinate dehydrogenase complex iron sulfur subunit B; COX4I1, Cytochrome *c* oxidase subunit 4I1; COX5B, Cytochrome *c* oxidase subunit 5B, COX6A1, Cytochrome *c* oxidase subunit 6A1; ATP5G2, ATP synthase membrane subunit c locus 2.

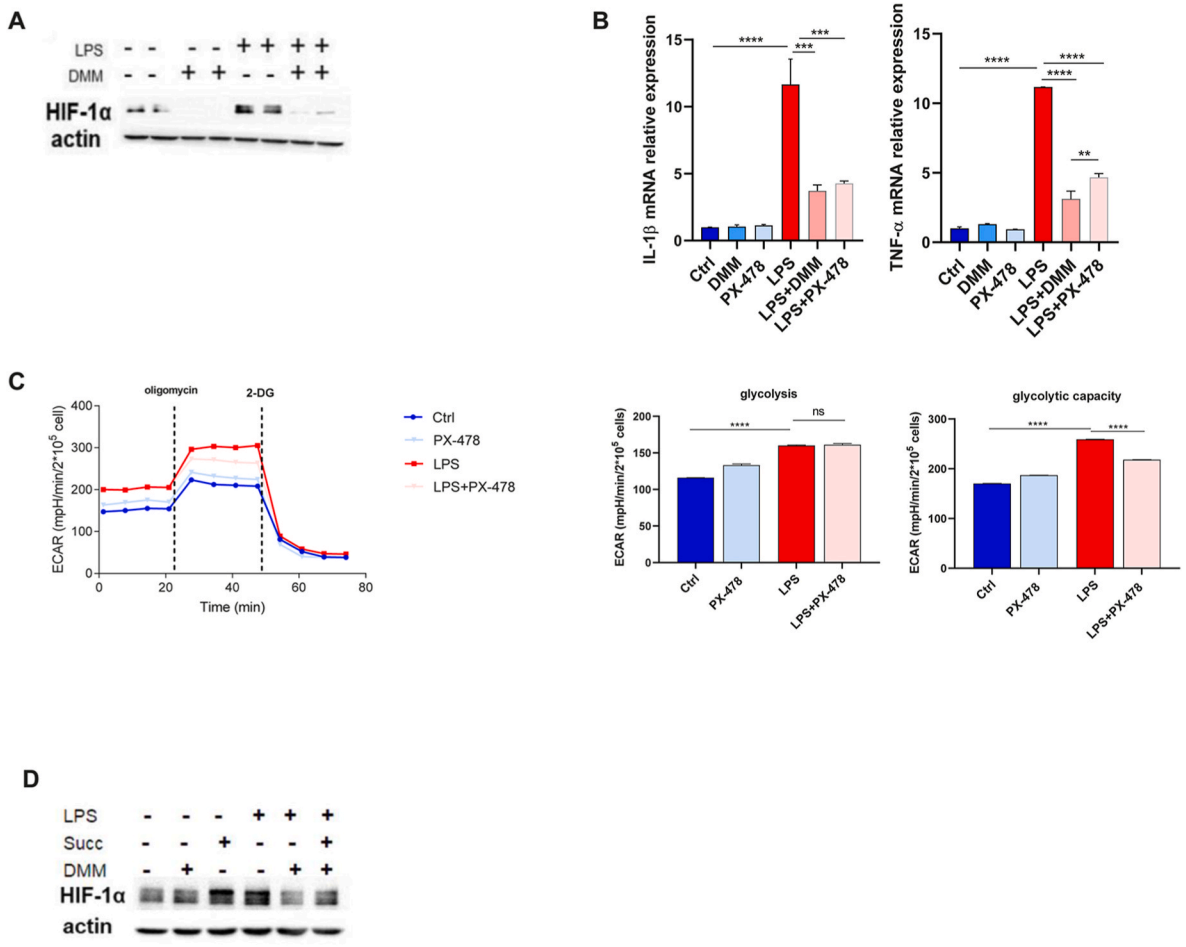

Fig. 4. HIF-1α is induced by SDH and partially mediates glycolysis enhancement and cytokine expression
(A) Representative pictures of protein levels of β-actin and HIF-1α determined by western blot analysis. HMC3 cells were treated for 24 h with LPS (1 μg/mL) +/- DMM (10 mM). (B) Relative mRNA expression of IL-1β and TNF-α in HMC3 treated with LPS (1 μg/mL), DMM (10 mM), and HIF-1α inhibitor (PX-478) (10 μM) for 24 h, determined by qPCR (n= 3 experiments performed in triplicate). (C) Glycolysis and glycolytic capacity determined by measuring ECAR in HMC3 treated with LPS, and PX-478 for 24h (n= 3 experiments performed in quadruplicate). (D) Representative pictures of protein levels of β-actin and HIF-1α determined by western blot analysis. HMC3 were pretreated for 3 h with diethyl succinate (5 mM) prior to stimulation with LPS (1 μg/mL) +/- DMM (10 mM) for 24 h. Data are expressed in mean ± SEM; **p < 0.01; ***p < 0.001, ****p < 0.0001 according to one-Way ANOVA followed by post hoc analysis (Bonferroni test). Il-1β, interleukin-1β; TNF-α, tumor necrosis factor-α; HIF-1α, hypoxia-Inducible factor-α; LPS, lipopolysaccharide; ECAR, extracellular acidification rate; Succ, diethyl succinate.

In a second step, performing a GO enrichment analysis we detected the top 20 significant terms for up-regulated genes in each category: cellular component (CC), molecular function (MF) and biological process (BP) (Fig. 6B–D). Intriguingly, in all GO categories there was a preponderant up-regulation of items involved in mitochondrial activity in 5xFAD microglia. For instance, in the CC ontology, we found "mitochondrial protein containing complex", "mitochondrial respirasome", "respiratory chain complex" (Fig. 6B). In the top 20 MF ontology terms we observed "electron transfer activity", "cytochrome c-oxidase activity", "proton transporting ATP-synthase activity" and several oxidoreductase activities (Fig. 6C). In accordance with this, analysing BP ontology we found that the second most significant term was "oxidative phosphorylation", followed by "cellular respiration" and "aerobic respiration". Several GO terms regarding mitochondrial respiratory chain complexes were represented in BP ontology (Fig. 6D). In addition to this, "Cytokine activity" term was also included in top 20 MF ontology (Fig. 6C).

Overall, these data underline that in a model of AD characterised by brain inflammation, microglia showed a peculiar transcriptome characterised by expression of several genes involved in mitochondrial respiration. In LPS-stimulated cells we have also described a high expression of genes encoding for ETC subunits. Therefore, we might speculate that in LPS-activated microglia and in AD mice microglia, the mitochondrial activity is supported at the transcriptional level.

3.6. *Microglia immunometabolism is a potential target in the early stages of AD, but not in advanced disease*

Finally, we questioned whether targeting microglia immunometabolism in advanced disease might still represent a potential strategy. In fact, we have already demonstrated that this AD model is characterized by inflammation, although cytokine expression progressively reduces during mice ageing [24]. Therefore, microglia were isolated from 18-months-aged 3xTg-AD mice and analysed. Interestingly, in contrast with results observed in 6-months-old mice, glycolysis and glycolytic capacity were reduced, although non significantly, (Fig. 7A), and basal and maximal respiration were significantly reduced in 3xTg-AD mice compared with controls (Fig. 7B). Moreover, DMM did not to exert any significant effect. Therefore, it is conceivable to believe that inflammation is an early determinant of AD pathogenesis, while in advanced disease, the neurodegeneration is consolidated, and microglia functions are inactivated. At this stage, targeting microglia inflammatory activity might be an unsuccessful strategy. In order to simulate this state of metabolic and inflammatory "exhaustion" *in vitro*, we exposed HMC3 to

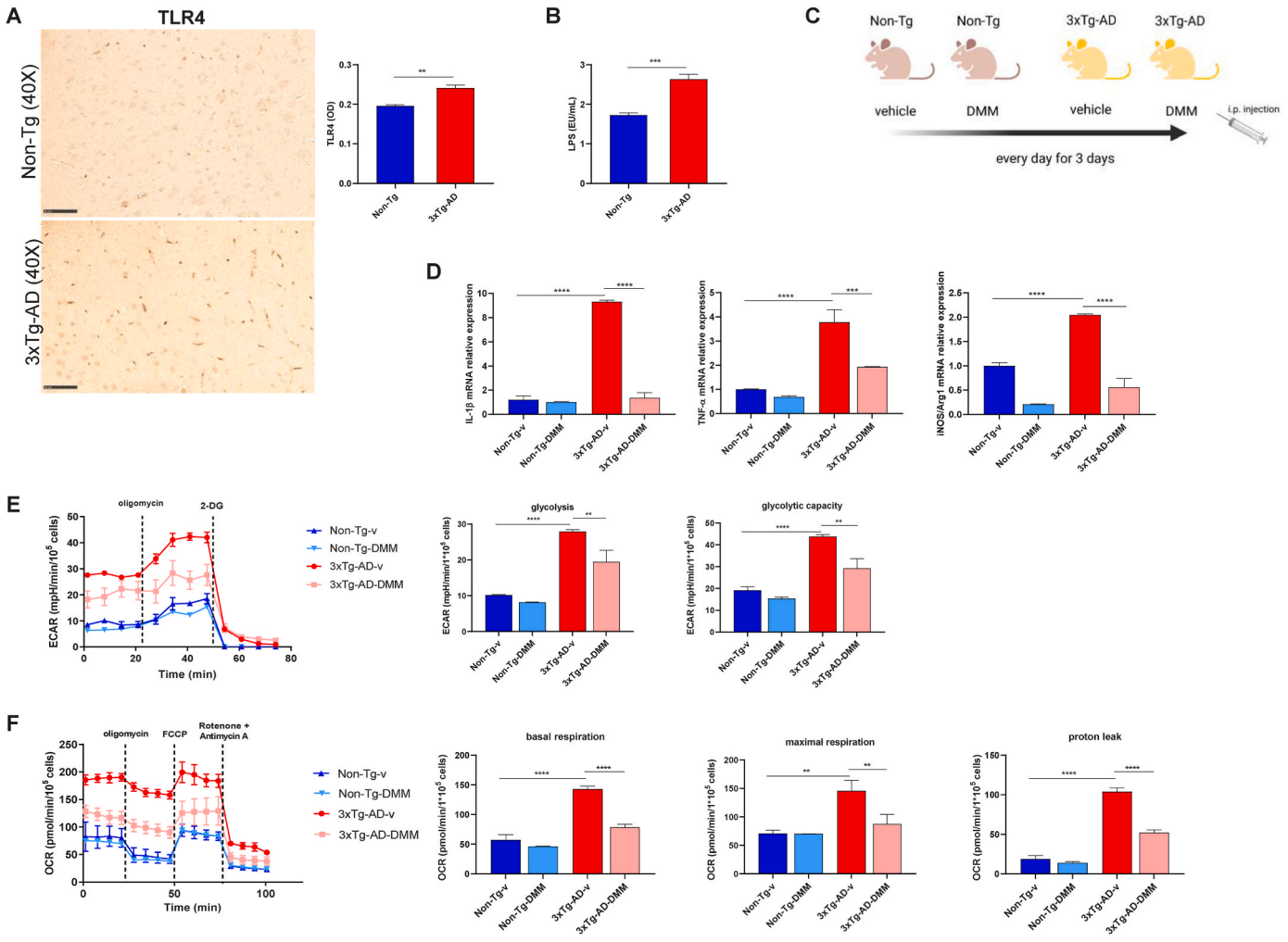

Fig. 5. Effects *in vivo* of SDH inhibition with DMM in 6-month-aged 3xTg-AD mice

(A) Representative pictures and quantification of TLR4 staining in cerebral cortices of Non-Tg and 3xTg-AD mice determined by immunohistochemistry (n= 4 per group). (B) Quantification of endotoxin (LPS) concentration in serum of Non-Tg and 3xTg-AD mice determined by using the Pierce™ Chromogenic Endotoxin Quant Kit (Thermo Fisher scientific) (n= 4 per group). (C) Experimental design. (D) Relative mRNA expression of Il-1β and TNF-α and iNOS/Arg1 ratio in cerebral cortices of 6-mo Non-Tg and 3xTg-AD mice intraperitoneally injected with vehicle (PBS) or DMM (160 mg/kg) for three days, and determined by qPCR (Non-Tg groups: n = 4; 3xTg-AD groups: n = 5). (E) Glycolysis and glycolytic capacity determined by measuring ECAR (Non-Tg groups: n= 4; 3xTg-AD groups: n = 6; each measurement performed in triplicate) and (F) mitochondrial respiration (basal, maximal and proton leak) determined by measuring OCR (Non-Tg groups: n= 3; 3xTg-AD: n = 4; each measurement performed in triplicate) in primary microglia cells isolated from 6-mo Non-Tg and 3xTg-AD mice intraperitoneally injected with vehicle (PBS) or DMM (160 mg/kg) for three days. Data are expressed in mean ± SEM; *p < 0.05; **p < 0.01; ***p < 0.001, ****p < 0.0001 according to one-Way ANOVA followed by post hoc analysis (Bonferroni test). TLR4, toll-like receptor 4; Il-1β, interleukin-1β; TNF-α, tumor necrosis factor-α; iNOS, inducible nitric oxide synthase; Arg1, arginase1; ECAR, extracellular acidification rate; OCR, oxygen consumption rate; DMM, dimethyl malonate.

LPS every day for 10 days and treated with DMM the last day only. Interestingly, both glycolytic capacity and maximal respiration were significantly reduced in LPS long-term exposed cells, and as expected, no relevant differences were found after DMM treatment (Fig. 7C and D). Taken together, our results underline the importance of targeting microglia immunometabolism in the early stages of AD.

4. Discussion

LPS-activated macrophages are characterized by enhanced glycolysis, a metabolic adaptation first observed in mouse peritoneal macrophages in 1970 [49]. More recently, several authors have reported other cellular metabolic changes in LPS-exposed macrophages, such as the decrease of OXPHOS and two important breaks occurring in the Krebs cycle: at isocitrate dehydrogenase (IDH), leading to citrate accumulation, and at SDH [49–51] with succinate accumulation. Beyond the metabolic switch from OXPHOS to glycolysis, the mitochondrial dysfunction has emerged as crucial in activated macrophages, revealing the central role of mitochondrial ROS in determining the production of pro-inflammatory cytokines [52,53]. Microglia, the resident immune cells of the central nervous system (CNS), have a metabolic similarity with macrophages since these cells reprogram their bioenergetic phenotype to support inflammation, although living in a peculiar microenvironment [54]. Few authors analysed the metabolic rewiring in microglia after LPS stimulation, but very little is known about underlying mechanisms, and to date potential applications have been only supposed [55]. In this study, we provide a model that explains different aspects of the metabolic rewiring in microglia after LPS exposure. Taken together, our findings suggest that TLR4-mediated activation of human microglia requires a peculiar bioenergetic phenotype which is governed by SDH activity, whose pharmacological inhibition might represent a valid therapeutic approach in AD. In particular, we observed that upon LPS exposure, microglia significantly increase the glycolytic activity and the mitochondrial respiration, although the latter is only partially

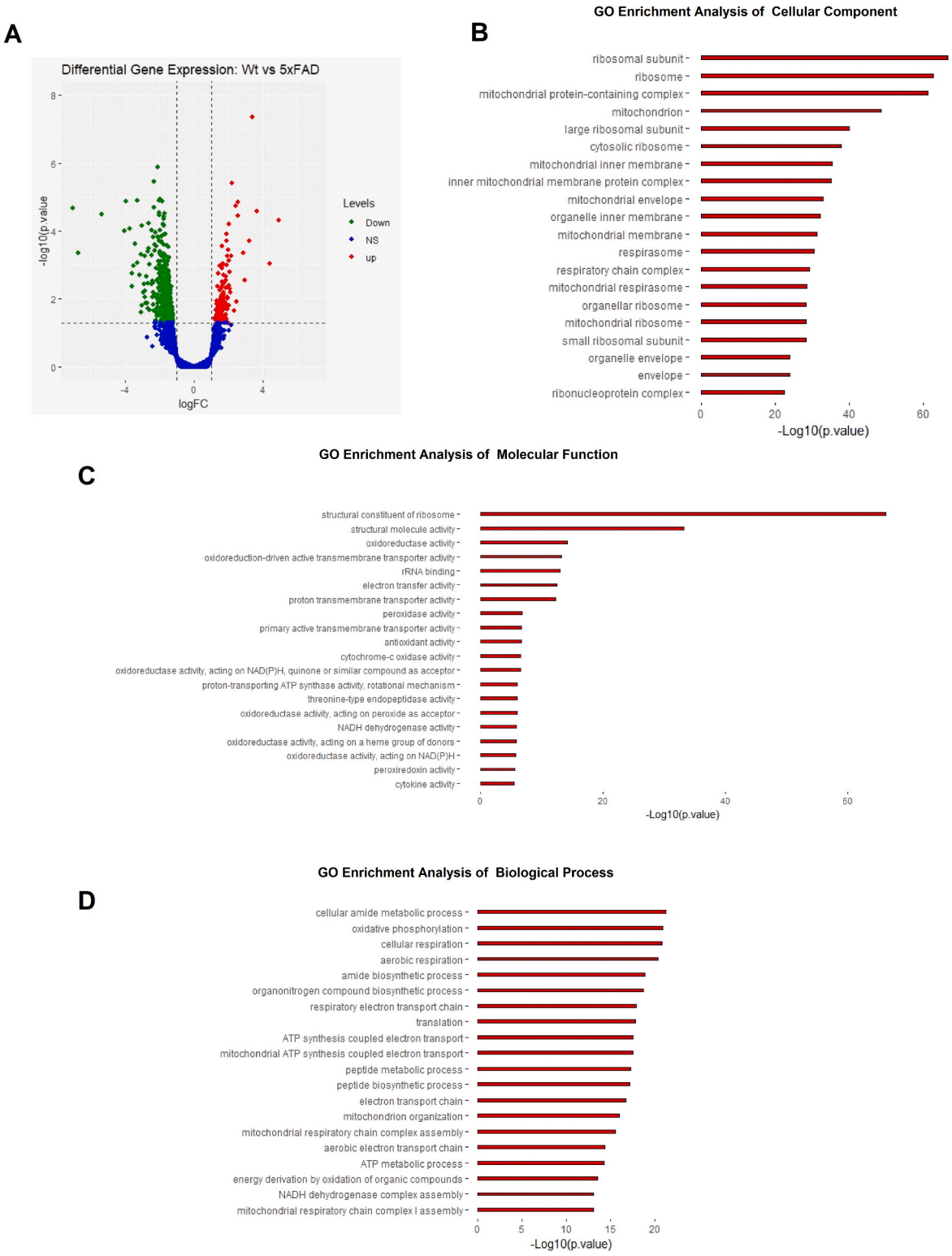

Fig. 6. Transcriptomic profile of microglia (WT vs 5xFAD mice) from public RNA-seq dataset
(A) Volcano Plot. (B–D) Top 20 terms from GO enrichment analysis of up-regulated genes, expressed in -Log10(p-value), for the three categories Cellular Component (CC), Molecular Function (MF) and Biological Process (BP). The analysis has been performed by downloaded public RNA-seq data (GSE231403; https://www.ncbi.nlm.nih.gov/geo/query/acc.cgi?acc=GSE231403), comparing transcriptomic profile of microglia from 3 WT mice vs 3 5xFAD mice.

devoted to ATP production with consequent proton leak and oxidative stress. In fact, whereas LPS boosted the enzymatic activity of ETC complex I and complex II, this was characterized by high rate of hydrogen peroxide production. Although different studies have demonstrated that LPS reduces macrophage ETC activity by inhibiting complexes I and II [56,57], Mills and O'Neill showed that LPS promotes complex I activity with consequent ROS production [58]; and the role of TLR4 on the modulation of complex I, whose dysfunction is frequently related to neurodegenerative disorders, has been recently emphasized in *Ndufs4*$^{-/-}$ mice [59]. In accordance, the complex I inhibition by

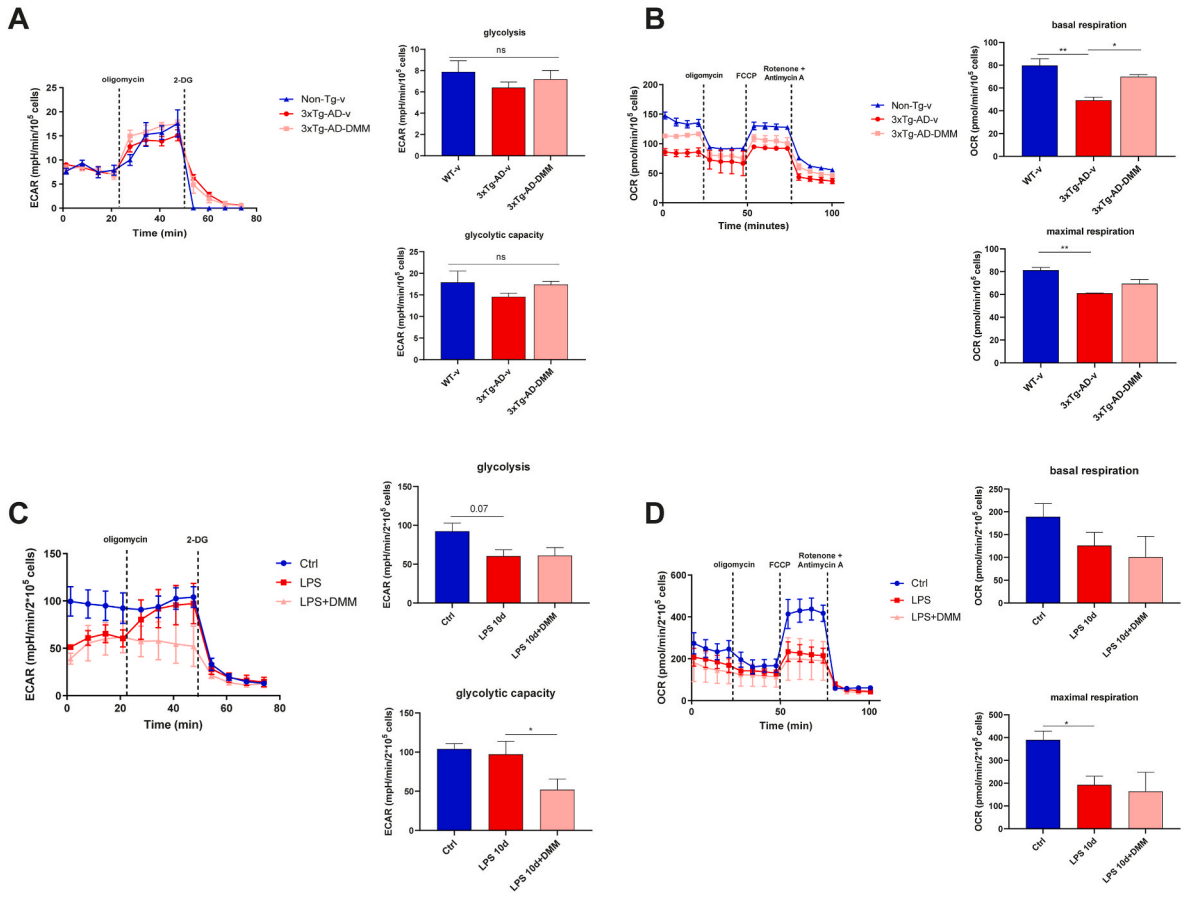

Fig. 7. Bioenergetic alterations in microglia of 18 month-aged 3xTg-AD mice and HMC3 after long-lasting LPS exposure
(A) Glycolysis and glycolytic capacity determined by measuring ECAR (Non-Tg group: n= 4; 3xTg-AD groups: n = 6; each measurement performed in triplicate) and (B) mitochondrial respiration (basal, maximal and proton leak) determined by measuring OCR (Non-Tg group: n= 3; 3xTg-AD groups: n = 4; each measurement performed in triplicate) in primary microglia isolated from 18-mo Non-Tg and 3xTg-AD mice intraperitoneally injected with vehicle (PBS) or DMM (160 mg/kg) for three days (C) Glycolysis and glycolytic capacity determined by measuring ECAR and (D) mitochondrial respiration (basal, maximal and proton leak) determined by measuring OCR in HMC3 cells treated with LPS (1 μg/mL) for 10 days ± DMM (10 mM) added the last 24h only (n = 3 per group; each measurement performed in quadruplicate). Data are expressed in mean ± SEM; *p < 0.05; **p < 0.01; ***p < 0.001, according to one-Way ANOVA followed by post hoc analysis (Bonferroni test).

metformin reduces IL-1β production in response to LPS [60]. Moreover, in line with our findings, recent evidence reported that LPS stimulation induces mitochondrial biogenesis in macrophages [61,62]. In our study, LPS induced the up-regulation of two important mitochondrial biogenesis markers (TFAM and PGC-1α) and of several ETC subunits. Therefore, it is conceivable that LPS further supports mitochondrial respiration by promoting mitochondrial biogenesis. Along with these observations, the treatment with DMM, an SDH inhibitor with anti-inflammatory properties [34,35], dampened IL-1β and TNF-α expression by reducing both glycolysis and mitochondrial respiration. In essence, by targeting SDH activity, DMM was able to counteract the LPS-induced mitochondrial biogenesis and dysfunction, hence the mitochondrial ROS generation. However, beyond these lines, the exact contribution of glycolysis and mitochondrial dysfunction to the cytokine expression, is unclear. Here, we observed that the DMM anti-inflammatory effect was progressively abolished by increasing the concentrations of glucose and H_2O_2, suggesting that both the glycolytic production of ATP and the oxidative stress facilitate inflammation. Accordingly, it is well known that the stoppage of glycolysis with 2-DG abrogates the IL-1β production in macrophages, whereas mitochondrial ROS contribute to cytokine production as well [63]. Moreover, the increase of ATP-synthase activity confirmed that ATP synthesis from OXPHOS is also required in active microglia. This is in agreement with a recent study where the administration of oligomycin (which completely stops ETC-derived ATP) reduced IL-1β production, suggesting a contribution of OXPHOS [20]. However, although the central role of SDH in microglia bioenergetic repurposing is clear, probably beyond the direct modulation of ETC activity, other indirect mechanisms exist. In a recent study, the HIF-1α suppression was suggested as a putative mediator of DMM action [20], as HIF-1α regulates the glycolytic metabolism and is involved in LPS-induced IL-1β production [37,39,64]. The authors assert that by inhibiting SDH, DMM restores ETC function, limiting the production of ROS, that otherwise would promote HIF-1α activity; on the other hand, other studies showed that SDH itself or oxidated succinate directly induces HIF-1α [39,42]. Here, we found that LPS-activated microglia expressed high levels of HIF-1α, which were normalized with DMM exposure. More importantly, treating cells with PX-478, a HIF-1α specific inhibitor, similarly to DMM, we obtained a significant cytokine down-regulation, and glycolytic capacity reduction. It is demonstrated that in macrophages HIF-1α is central in determining transcription for glycolysis, although not exclusive as other mechanisms contribute in a complex cross-talk between glycolysis enzymes and transcription factors [64]. For instance, recently an alternative mechanism has been proposed where glycerol phosphate shuttle enzyme (GPD2) drives glucose oxidation and inflammatory mediator transcription in macrophages upon LPS exposure [47]. In accordance with this, in our study, DMM was able to inhibit both IL-1β and TNF-α expression, and HIF-1α inhibition replicated the anti-inflammatory effect of DMM,

although with a lower impact on TNF-α. These findings suggest that, in microglia, SDH activity regulates glycolysis and cytokine production via HIF-1α, but these might also rely on other mechanisms. It is usually reported that HIF-1α modulates IL-1β expression with no effect on TNF-α [39]; on the other hand, it has also been reported that HIF-1α induces TNF-α expression in macrophages [65].

Collectively, these data have indicated that the endosymbiotic origin of mitochondria is linked not only to the requirement of eukaryotes to have a cell "powerhouse", involved in ATP production. These organelles evolved by integrating as a cellular hub with the role of coordinating a complex network of signals, constituted by the variation of metabolic pathways and metabolites, by which specific functions and cell fate are determined. Finally, using an AD murine model, the 3xTg-AD, that develops Aβ plaques and NFTs in an age- and region-dependent manner, highly mimicking the development of AD in the human brain [22–24], we showed that early stages of AD are characterised by an inflammatory state with high TLR4-expressing microglia. Some studies have shown high LPS levels in patients with AD both in blood and in the brain, and LPS-induced TLR4 activation has been proposed as important mediator of brain inflammation in amyloid pathology [10,11]. Here, we found high levels of circulating LPS in 3xTg-AD mice. On the other hand, recent studies demonstrated that Aβ can also activate microglia via TLR4 [12]. Therefore, we have also analysed the effects of Aβ exposure on HMC3, finding a proinflammatory effect and a metabolic reprogramming profile very similar to the LPS-induced one. Furthermore, the treatment with TAK-242, a selective inhibitor of TLR4, abrogated the Aβ effects, suggesting that Aβ behaves as a TLR4 activator. However, compared to LPS the Aβ action was weaker and not sufficient to justify the considerable changes of microglia observed in 3xTg-AD mice. Therefore, we can hypothesize that both Aβ and circulating LPS, are essential triggers of microglia activation in AD patients, perhaps cooperating at co-receptor level. Further investigations are needed to clarify this point.

It was interesting to note that similarly to LPS-stimulated human cells, inflammatory microglia from AD mice were supported by a metabolic rewiring with a considerable increase of glycolysis and mitochondrial respiration, with a very high proton leak. The analysis performed on RNA-seq public data, comparing microglia of WT mice vs 5xFAD mice, described a strong up-regulation of several pathways involved in mitochondrial respiration in AD mice. This was in line with our above-mentioned observation where ETC subunit gene expression was induced by LPS, corroborating the hypothesis that TLR4-mediated activation in microglia requires mitochondrial biogenesis to support the increase of respiration. However, despite the *in vitro* and *in vivo* analyses, we are still not able to describe the effectors which link the SDH activity with the transcription of mitochondrial subunits. Some evidence in other cell types recently demonstrated a very complex interaction between SDH activity and several RNA networks including non-coding RNAs, RNA editors, and RNA modifiers, which would link SDH activity to a transcriptional profile [66]. On the other hand, several HIFs protein, activated by SDH, seem to regulate several functions including mitochondrial biogenesis [67]. Overall, we believe that the mechanisms are multiple and complex, involving nc-RNAs, HIFs protein, energetic sensors, ATP, NADH and others.

Moreover, SDH inhibition by DMM administration *in vivo* revealed an effective strategy to control microglia bioenergetic reprogramming and dampen inflammation in AD. The efficacy of DMM *in vivo* would suggest that oxidative stress at early stages of AD derives from microglia ROS production. On the contrary, in advanced disease, when inflammation is extinguished [47], microglia presented a sort of metabolic "exhaustion" likely due to a long-lasting activation state. Here, targeting SDH resulted inappropriate.

In conclusion, TLR4 activation promotes metabolic changes and proinflammatory activity in microglia, and SDH might represent a promising therapeutic target to control inflammation at early stages of AD.

Author contribution

M.S. and M.C. designed and performed experiments, analysed data, and wrote the manuscript. T.C. contributed to the study design and performed *in vivo* experiments, providing 3-Tg-AD mice. A.R. helped with experimentations and performed analysis of RN-seq dataset. A.M., V.N.S., A.R., R.V. and H.K, helped to perform *in vitro* and *in vivo* experiments and data analysis. L.D. performed and analysed histology and provided microscopy pictures; N.C. contributed with critical analysis and suggestions; C.A. provided technical advice for *in vitro* experiments; G.S. supervised the entire project, provided conceptual means, and drafted the manuscript.

Funding

The work was supported by the publication funding of Department of Medical and Surgical Sciences, University of Foggia, Italy.

Declaration of competing interest

The authors declare that they have no known competing financial interests or personal relationships that could have appeared to influence the work reported in this paper.

Appendix A. Supplementary data

Supplementary data to this article can be found online at https://doi.org/10.1016/j.redox.2023.102846.

References

[1] L. Mucke, Neuroscience: Alzheimer's disease, Nature 461 (2009) 895–897.
[2] H.S. Kwon, S.H. Koh, Neuroinflammation in neurodegenerative disorders: the roles of microglia and astrocytes, Transl. Neurodegener. 9 (2020) 42.
[3] J. Yang, L. Wise, K.I. Fukuchi, TLR4 cross-talk with NLRP3 inflammasome and complement signaling pathways in Alzheimer's disease, Front. Immunol. 11 (2020) 724.
[4] M. Calvo-Rodriguez, C. Garcia-Rodriguez, C. Villalobos, et al., Role of toll like receptor 4 in Alzheimer's disease, Front. Immunol. 11 (2020) 1588.
[5] P. d'Errico, S. Ziegler-Waldkirch, V. Aires, et al., Microglia contribute to the propagation of Abeta into unaffected brain tissue, Nat. Neurosci. 25 (2022) 20–25.
[6] B.S. Park, J.O. Lee, Recognition of lipopolysaccharide pattern by TLR4 complexes, Exp. Mol. Med. 45 (2013) e66.
[7] E. Lien, T.K. Means, H. Heine, et al., Toll-like receptor 4 imparts ligand-specific recognition of bacterial lipopolysaccharide, J. Clin. Invest. 105 (2000) 497–504.
[8] S. Walter, M. Letiembre, Y. Liu, et al., Role of the toll-like receptor 4 in neuroinflammation in Alzheimer's disease, Cell. Physiol. Biochem. 20 (2007) 947–956.
[9] M. Zhu, X. Wang, M. Schultzberg, et al., Differential regulation of resolution in inflammation induced by amyloid-beta42 and lipopolysaccharides in human microglia, J Alzheimers Dis 43 (2015) 1237–1250.
[10] M. Marizzoni, A. Cattaneo, P. Mirabelli, et al., Short-chain fatty acids and lipopolysaccharide as mediators between gut dysbiosis and amyloid pathology in Alzheimer's disease, J Alzheimers Dis 78 (2020) 683–697.
[11] X. Zhan, B. Stamova, F.R. Sharp, Lipopolysaccharide associates with amyloid plaques, neurons and oligodendrocytes in Alzheimer's disease brain: a review, Front. Aging Neurosci. 10 (2018) 42.
[12] Y. Zhou, Y. Chen, C. Xu, et al., TLR4 targeting as a promising therapeutic strategy for alzheimer disease treatment, Front. Neurosci. 14 (2020), 602508.
[13] R. Villani, M. Sangineto, P. Pontrelli, et al., Eradication of HCV by direct antiviral agents restores mitochondrial function and energy homeostasis in peripheral blood mononuclear cells, Faseb. J. 36 (2022), e22650.
[14] J. Van den Bossche, L.A. O'Neill, D. Menon, Macrophage immunometabolism: where are we (going)? Trends Immunol. 38 (2017) 395–406.
[15] L.A. O'Neill, R.J. Kishton, J. Rathmell, A guide to immunometabolism for immunologists, Nat. Rev. Immunol. 16 (2016) 553–565.
[16] https://www.atcc.org/products/crl-3304.
[17] M. Baek, E. Yoo, H.I. Choi, et al., The BET inhibitor attenuates the inflammatory response and cell migration in human microglial HMC3 cell line, Sci. Rep. 11 (2021) 8828.
[18] C. Dello Russo, N. Cappoli, I. Coletta, et al., The human microglial HMC3 cell line: where do we stand? A systematic literature review, J. Neuroinflammation 15 (2018) 259.
[19] D. Gosselin, D. Skola, N.G. Coufal, et al., An environment-dependent transcriptional network specifies human microglia identity, Science 356 (2017).

[20] E.L. Mills, B. Kelly, A. Logan, et al., Succinate dehydrogenase supports metabolic repurposing of mitochondria to drive inflammatory macrophages, Cell 167 (2016) 457–470 e13.
[21] K. Shabir, S. Gharanei, S. Orton, et al., Asprosin exerts pro-inflammatory effects in THP-1 macrophages mediated via the toll-like receptor 4 (TLR4) pathway, Int. J. Mol. Sci. (2022) 24.
[22] T. Cassano, A. Romano, T. Macheda, et al., Olfactory memory is impaired in a triple transgenic model of Alzheimer disease, Behav. Brain Res. 224 (2011) 408–412.
[23] S. Oddo, A. Caccamo, M. Kitazawa, et al., Amyloid deposition precedes tangle formation in a triple transgenic model of Alzheimer's disease, Neurobiol. Aging 24 (2003) 1063–1070.
[24] C. Scuderi, M.R. Bronzuoli, R. Facchinetti, et al., Ultramicronized palmitoylethanolamide rescues learning and memory impairments in a triple transgenic mouse model of Alzheimer's disease by exerting anti-inflammatory and neuroprotective effects, Transl. Psychiatry 8 (2018) 32.
[25] T. Cassano, A. Magini, S. Giovagnoli, et al., Early intrathecal infusion of everolimus restores cognitive function and mood in a murine model of Alzheimer's disease, Exp. Neurol. 311 (2019) 88–105.
[26] T. Cassano, F. Giamogante, S. Calcagnini, et al., PDIA3 expression is altered in the limbic brain regions of triple-transgenic mouse model of Alzheimer's disease, Int. J. Mol. Sci. (2023) 24.
[27] J.K. Lee, M.G. Tansey, Microglia isolation from adult mouse brain, Methods Mol. Biol. 1041 (2013) 17–23.
[28] M. Sangineto, V.N. Bukke, F. Bellanti, et al., A novel nutraceuticals mixture improves liver steatosis by preventing oxidative stress and mitochondrial dysfunction in a NAFLD model, Nutrients 13 (2021).
[29] A.J. Janssen, F.J. Trijbels, R.C. Sengers, et al., Spectrophotometric assay for complex I of the respiratory chain in tissue samples and cultured fibroblasts, Clin. Chem. 53 (2007) 729–734.
[30] F. Bellanti, R. Villani, R. Tamborra, et al., Synergistic interaction of fatty acids and oxysterols impairs mitochondrial function and limits liver adaptation during nafld progression, Redox Biol. 15 (2018) 86–96.
[31] A. Barrientos, In vivo and in organello assessment of OXPHOS activities, Methods 26 (2002) 307–316.
[32] F. Bellanti, A.D. Romano, A.M. Giudetti, et al., Many faces of mitochondrial uncoupling during age: damage or defense? J Gerontol A Biol Sci Med Sci 68 (2013) 892–902.
[33] M. Tsuchida, T. Miura, K. Mizutani, et al., Fluorescent substances in mouse and human sera as a parameter of in vivo lipid peroxidation, Biochim. Biophys. Acta 834 (1985) 196–204.
[34] Q. Yu, Y. Wang, L. Dong, et al., Regulations of glycolytic activities on macrophages functions in tumor and infectious inflammation, Front. Cell. Infect. Microbiol. 10 (2020) 287.
[35] Y. Yang, R. Shao, L. Tang, et al., Succinate dehydrogenase inhibitor dimethyl malonate alleviates LPS/d-galactosamine-induced acute hepatic damage in mice, Innate Immun. 25 (2019) 522–529.
[36] M. Ii, N. Matsunaga, K. Hazeki, et al., A novel cyclohexene derivative, ethyl (6R)-6-[N-(2-Chloro-4-fluorophenyl)sulfamoyl]cyclohex-1-ene-1-carboxylate (TAK-242), selectively inhibits toll-like receptor 4-mediated cytokine production through suppression of intracellular signaling, Mol. Pharmacol. 69 (2006) 1288–1295.
[37] C.C. Blouin, E.L. Page, G.M. Soucy, et al., Hypoxic gene activation by lipopolysaccharide in macrophages: implication of hypoxia-inducible factor 1alpha, Blood 103 (2004) 1124–1130.
[38] E.M. Palsson-McDermott, A.M. Curtis, G. Goel, et al., Pyruvate kinase M2 regulates Hif-1alpha activity and IL-1beta induction and is a critical determinant of the warburg effect in LPS-activated macrophages, Cell Metabol. 21 (2015) 65–80.
[39] G.M. Tannahill, A.M. Curtis, J. Adamik, et al., Succinate is an inflammatory signal that induces IL-1beta through HIF-1alpha, Nature 496 (2013) 238–242.
[40] K. Lee, H.M. Kim, A novel approach to cancer therapy using PX-478 as a HIF-1alpha inhibitor, Arch Pharm. Res. (Seoul) 34 (2011) 1583–1585.
[41] N. Villa-Roel, K. Ryu, L. Gu, et al., Hypoxia inducible factor 1alpha inhibitor PX-478 reduces atherosclerosis in mice, Atherosclerosis 344 (2022) 20–30.
[42] S.E. Corcoran, L.A. O'Neill, HIF1alpha and metabolic reprogramming in inflammation, J. Clin. Invest. 126 (2016) 3699–3707.
[43] D.V. Hansen, J.E. Hanson, M. Sheng, Microglia in Alzheimer's disease, J. Cell Biol. 217 (2018) 459–472.
[44] E. Gatta, T. Lefebvre, S. Gaetani, et al., Evidence for an imbalance between tau O-GlcNAcylation and phosphorylation in the hippocampus of a mouse model of Alzheimer's disease, Pharmacol. Res. 105 (2016) 186–197.
[45] F. Bellanti, V.N. Bukke, A. Moola, et al., Effects of ultramicronized palmitoylethanolamide on mitochondrial bioenergetics, cerebral metabolism, and glutamatergic transmission: an integrated approach in a triple transgenic mouse model of Alzheimer's disease, Front. Aging Neurosci. 14 (2022), 890855.
[46] E. Barone, F. Di Domenico, T. Cassano, et al., Impairment of biliverdin reductase-A promotes brain insulin resistance in Alzheimer disease: a new paradigm, Free Radic. Biol. Med. 91 (2016) 127–142.
[47] V. Landel, K. Baranger, I. Virard, et al., Temporal gene profiling of the 5XFAD transgenic mouse model highlights the importance of microglial activation in Alzheimer's disease, Mol. Neurodegener. 9 (2014) 33.
[48] C.C. Liu, C.C. Liu, T. Kanekiyo, et al., Apolipoprotein E and Alzheimer disease: risk, mechanisms and therapy, Nat. Rev. Neurol. 9 (2013) 106–118.
[49] G.C. Hard, Some biochemical aspects of the immune macrophage, Br. J. Exp. Pathol. 51 (1970) 97–105.
[50] A.K. Jha, S.C. Huang, A. Sergushichev, et al., Network integration of parallel metabolic and transcriptional data reveals metabolic modules that regulate macrophage polarization, Immunity 42 (2015) 419–430.
[51] A. Marrocco, L.A. Ortiz, Role of metabolic reprogramming in pro-inflammatory cytokine secretion from LPS or silica-activated macrophages, Front. Immunol. 13 (2022), 936167.
[52] A.C. Bulua, A. Simon, R. Maddipati, et al., Mitochondrial reactive oxygen species promote production of proinflammatory cytokines and are elevated in TNFR1-associated periodic syndrome (TRAPS), J. Exp. Med. 208 (2011) 519–533.
[53] A.P. West, I.E. Brodsky, C. Rahner, et al., TLR signalling augments macrophage bactericidal activity through mitochondrial ROS, Nature 472 (2011) 476–480.
[54] S. Ghosh, E. Castillo, E.S. Frias, et al., Bioenergetic regulation of microglia, Glia 66 (2018) 1200–1212.
[55] C. Lauro, C. Limatola, Metabolic reprograming of microglia in the regulation of the innate inflammatory response, Front. Immunol. 11 (2020) 493.
[56] M. Kato, Site of action of lipid A on mitochondria, J. Bacteriol. 112 (1972) 268–275.
[57] A. McGivney, S.G. Bradley, Action of bacterial endotoxin and lipid A on mitochondrial enzyme activities of cells in culture and subcellular fractions, Infect. Immun. 25 (1979) 664–671.
[58] E.L. Mills, L.A. O'Neill, Reprogramming mitochondrial metabolism in macrophages as an anti-inflammatory signal, Eur. J. Immunol. 46 (2016) 13–21.
[59] Z. Jin, W. Wei, M. Yang, et al., Mitochondrial complex I activity suppresses inflammation and enhances bone resorption by shifting macrophage-osteoclast polarization, Cell Metabol. 20 (2014) 483–498.
[60] B. Kelly, G.M. Tannahill, M.P. Murphy, et al., Metformin inhibits the production of reactive oxygen species from NADH:ubiquinone oxidoreductase to limit induction of interleukin-1beta (IL-1beta) and boosts interleukin-10 (IL-10) in lipopolysaccharide (LPS)-activated macrophages, J. Biol. Chem. 290 (2015) 20348–20359.
[61] R. Kapetanovic, S.F. Afroz, D. Ramnath, et al., Lipopolysaccharide promotes Drp1-dependent mitochondrial fission and associated inflammatory responses in macrophages, Immunol. Cell Biol. 98 (2020) 528–539.
[62] W. Yu, X. Wang, J. Zhao, et al., Stat2-Drp1 mediated mitochondrial mass increase is necessary for pro-inflammatory differentiation of macrophages, Redox Biol. 37 (2020), 101761.
[63] M. Canton, R. Sanchez-Rodriguez, I. Spera, et al., Reactive oxygen species in macrophages: sources and targets, Front. Immunol. 12 (2021), 734229.
[64] G. Soto-Heredero, M.M. Gomez de Las Heras, E. Gabande-Rodriguez, et al., Glycolysis - a key player in the inflammatory response, FEBS J. 287 (2020) 3350–3369.
[65] A. Lewis, P.M. Elks, Hypoxia induces macrophage tnfa expression via cyclooxygenase and prostaglandin E2 in vivo, Front. Immunol. 10 (2019) 2321.
[66] C. Moreno, R.M. Santos, R. Burns, et al., Succinate dehydrogenase and ribonucleic acid networks in cancer and other diseases, Cancers 12 (2020).
[67] X. Bao, J. Zhang, G. Huang, et al., The crosstalk between HIFs and mitochondrial dysfunctions in cancer development, Cell Death Dis. 12 (2021) 215.